Hydrological Response to Vegetation Changes in the Yellow River Basin

Z. J. Wang[1], M. Z. Xu[1], G. Penny[2], H. C. Hu[1] , and X. P. Zhang[3]

[1]State Key Laboratory of Hydroscience and Engineering, Tsinghua University, Beijing, China

[2]Department of Geography, National University of Singapore, Singapore, Singapore

[3]Yellow River Institute of Hydraulic Research, MWR, Zhengzhou 450003, China

Corresponding author: M. Z. Xu (mzxu@mail.tsinghua.edu.cn)

Key Points:

- A novel vegetation-based analysis framework for water-food-ecology nexus was proposed
- Distributed Budyko-based hydrological analysis was realized with ERA5-Land dataset
- Climate change and ecological engineering magnified agricultural vulnerability in the Yellow River Basin

Abstract

The Yellow River Basin (YRB) is confronted with significant conflicts between water, food, and ecology. A thorough understanding of the human stresses on eco-hydrological processes is essential for the sustainable management of the YRB. To simplify the complex nature-human interaction system, we developed an analysis framework based on vegetation change and the Budyko hypothesis. The intra-annual vegetation change was explored using phenological indicators, in addition to the inter-annual vegetation change represented by annual maximum NDVI. K-means clustering was used to identify seven patterns of vegetation change driven by different ecological projects, agricultural alterations, and climate change. To explore the hydrological responses to environmental changes revealed by vegetation, a distributed attribution analysis of runoff changes was conducted using the ERA5-Land dataset and an elasticity method based on the Budyko hypothesis. The results show that the hydrological-related landscape changed most in the semi-humid and semi-arid areas experiencing revegetation, and the aridity increased most in the upstream and downstream irrigation areas. Human-driven landscape changes contributed to 44.1% - 60.7% of the local runoff reduction within the YRB. Notably, agricultural changes intensified drought, similar to revegetation, and meanwhile, the combined effect of climate change and ecological engineering could magnify agricultural vulnerability. We propose the adoption of drought-tolerant crop planting and water transfer across watersheds to ensure water-food-ecology security.

1 Introduction

The world's major rivers and their floodplains are crucial for economic development and support some of the most diverse habitats on the planet. However, their sustainability is increasingly challenged by anthropogenic stressors (Best, 2018). Establishing an inclusive governance framework across regions, scales, organizations, and local communities in large river basins requires a comprehensive understanding of nature-human interaction systems. However, this is challenging due to the complexity and substantial differences across the major river basins (Karabulut et al., 2016). The Yellow River Basin (YRB), known as the birthplace of Chinese civilization, is experiencing a severe conflict between development and protection, constrained by limited water resources, fragile ecosystems, and long-term anthropogenic stressors (Chen et al., 2015; Wang et al., 2015). With annual water resources of 64.7 billion m^3, less than 7% of the Yangtze River, the YRB is home to a population of 160 million people. The utilization rate of water resources in the YRB has reached 80%, well beyond sustainable limits which are typically considered to be about 40% (the State Council, 2021). Ecological protection and high-quality development in the YRB have been designated as a national strategy since 2019.

Vegetation is a critical component of the global water and carbon cycle (Gerten et al., 2004; Pan et al., 2011), and serves as a crucial indicator of environmental change (Root et al., 2003). The Yellow River Basin (YRB) is an area where vegetation has been significantly impacted by both long-term agricultural activities and large-scale ecological engineering initiatives. Historical records show that forests in the YRB were converted to farmland starting around AD 1000, which increased erosion and annual sediment delivery to the Yellow River over multiple centuries, culminating in a peak sediment discharge of about 1.6 Gt in the 1950s (Ren, 2006). To address the soil erosion issue, the Grain for Green Project was initiated in 1999, which is the world's largest active revegetation program. As a result, vegetation coverage on the Loess Plateau increased from 31.6% in 1999 to 59.6% in 2013 (Chen et al., 2015). Following the rapid greening, the annual sediment load decreased to the pristine level of about 0.2 Gt.

However, vegetation expansion has created potential water demand conflicts between ecosystems and humans in water-limited areas (Feng et al., 2016). Conservation measures to mitigate soil erosion have led to a runoff reduction of 0.25 $km^3\ yr^{-1}$ from the 1950s to the 2010s, exacerbating water scarcity in the YRB (Wang et al., 2015; Yang et al., 2004). Furthermore, the reduction in agriculture due to vegetation expansion may result in food deficits, which could be a significant concern for Chinese food security, as food production of YRB accounts for about one-third of the country's output (Chen et al., 2015). In addition to ecological engineering, agricultural mechanization and water-conservation reforms have also significantly impacted the croplands in the YRB in the past few decades. Therefore, vegetation changes in the YRB can serve as an indicator of the impact of agricultural activities, ecological engineering, and climate change on water, food, and ecosystems. Studying vegetation changes and their corresponding hydrological responses could provide a breakthrough in simplifying the complicated multi-factor relationships in the large-scale YRB.

Methodologically, various methods have been employed to study the hydrological impacts of climate change and human activities in the Yellow River Basin (YRB), including statistical regression methods, elastic methods, and physical models (Kong et al., 2016). Among these, simple linear regression and double mass curve methods are commonly used statistical methods that divide time series into baseline and changing periods to establish the relationship between precipitation and discharge/sediment load to detect the effects of climate change and anthropogenic activities (Gao et al., 2017; Zhao et al., 2018). Elasticity methods used in the YRB are usually based on the Budyko framework, which considers both water and energy constraints in hydrological processes over a long-term period (Budyko, 1974; Li et al., 2019; Xu et al., 2014). Most statistical regression methods and elasticity methods, which are lumped and easily applicable, ignore spatial heterogeneity and assume uniformity of hydrological variables and parameters in an entire basin (Wang et al., 2022). Recently developed physical hydrological models are distributed and have finer temporal and spatial resolutions (Yang et al., 2000), applying varying parameters for different meshes to simulate and predict site-specific variations over different time scales (Liu et al., 2019; Lu et al., 2020). However, these models are limited by their complex structures, large numbers of input datasets, time requirements, and uncertainty in model calibration and validation (Gao et al., 2016). Furthermore, most physical models still require the calibration of empirical coefficients (Wu et al., 2018).

We aim to bridge this technical research gap by using model-based meteorological reanalysis data instead of station data in the application of an elasticity method based on the Budyko hypothesis. Model-based meteorological products have undergone rapid development over the past few decades (Muñoz-Sabater et al., 2021). The state-of-the-art model-based dataset, ERA5-land, has been verified to have a good performance over subregions of temperate monsoon climate and temperate continental climate in China, which is the major type of the YRB (Xin et al., 2022; Xu et al., 2022). The use of ERA5-land enables a continuous and accurate representation of spatial meteorological heterogeneity, as well as the provision of additional surface indicators such as evaporation, which allows for the distributed Budyko analysis to present the runoff analysis results that are comparable to those obtained in physical models. Moreover, the proposed analysis method is easier to apply than distributed physical models, while retaining a stronger physical foundation than statistical methods.

With the increasing conflict between water, food, and ecosystems in the YRB, it is urgent to gain a better understanding of the complex eco-hydrological processes impacted by human activities to promote sustainable river management. Vegetation change serves as a useful indicator of environmental changes and can help to simplify the relationships between water, food, and ecosystems. Specifically, our objectives are to (a) characterize vegetation change patterns and their drivers across the YRB, (b) quantify the impact of different vegetation changes on runoff, and (c) provide recommendations for alleviating water-food-ecology conflicts in the YRB.

2 Materials and Methods

2.1 Study sites

The Yellow River, originating from the Qinghai-Tibet Plateau and draining into the Bohai Sea, is one of the longest rivers in China, with a length of 5464 km and an area of 7.95×10^5 km^2. The climate in the basin varies from humid in the southeast to arid in the northwest, with a corresponding decrease in precipitation from the southeast to the northwest. To facilitate analysis, the Yellow River Basin (YRB) has been divided into seven sections based on seven key hydrological stations on the mainstream (Figure 1, Table 1). S1, located upstream of Tangnaihai, is the source region of the Yellow River, with an average altitude of over 4000 m. S2 (Tangnaihai - Lanzhou) is a transition zone with a steep slope and super-large reservoirs. S3 (Lanzhou - Toudaoguai) is on the Inner Mongolia Plateau, with an altitude of 1000-2000 m. S4 (Toudaoguai - Longmen) and S5 (Longmen-Sanmenxia) are located on the Loess Plateau and experience severe soil erosion. S6 (Sanmenxia - Huayuankou) is another terrain transition zone, descending from an altitude of ~ 1000 m to ~ 95 m, and also has massive reservoirs to regulate the Yellow River's runoff and sediment load. S7 (Huayuankou - Lijin) is characterized by a flat alluvial plain with a strong depositional tendency. The YRB's diverse climate, landforms, and long-term human activities have led to various vegetation types in the region.

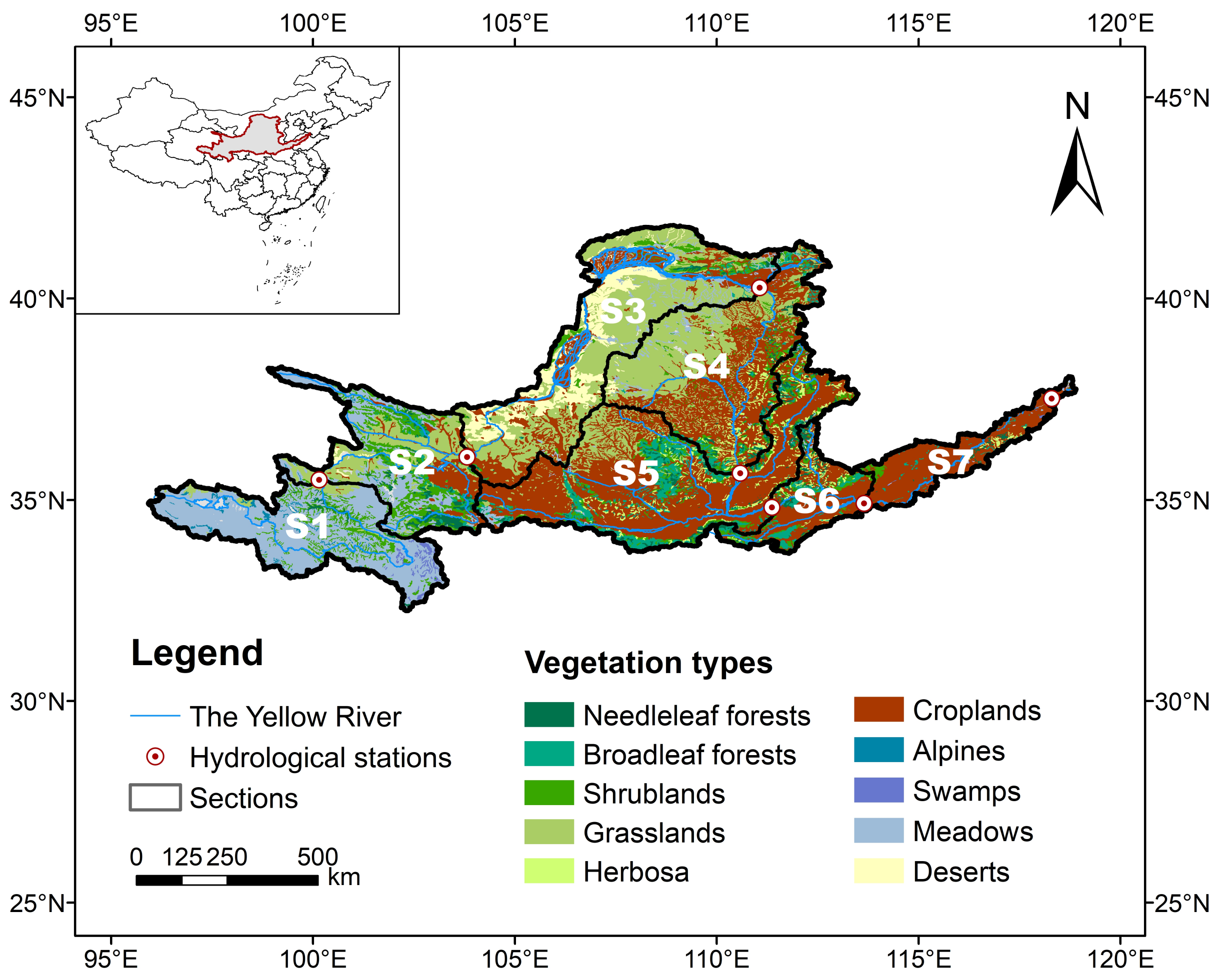

Figure 1 Map of the seven sections and vegetation types in the Yellow River Basin

Table 1 Characteristics of the seven sections in the Yellow River Basin

Section	Inlet station	Outlet station	Area (10^3 km^2)	Major vegetation types
S1	-	Tangnaihai	114	meadows (75.8%), shrublands (10.9%), grasslands (5.2%)
S2	Tangnaihai	Lanzhou	105	meadows (28.4%), grasslands (26.0%), shrublands (20.84%)
S3	Lanzhou	Toudaoguai	171	grasslands (45.5%), croplands (23.2%), deserts (19.2%)
S4	Toudaoguai	Longmen	153	croplands (43.2%), grasslands (38.6%), shrublands (5.5%)
S5	Longmen	Sanmenxia	199	croplands (62.6%), broadleaf forests (10.5%), grasslands (8.1%)
S6	Sanmenxia	Huayuankou	49	croplands (57.3%), broadleaf forests (14.9%), shrublands (10.5%)
S7	Huayuankou	Lijin	51	croplands (85.9%), shrublands (3.34%), broadleaf forests (2.67%)

2.2 Methodologies

With the vegetation-based idea, we developed an integrated framework for data analysis (Figure 2). Firstly, we analyzed the inter-annual and intra-annual changes of NDVI in the YRB. To be specific, we extracted the time sequence of four vegetation indicators, namely the annual maximum (NDVImax), start-of-season (SOS), end-of-season (EOS), and growing season length (GSL) of each pixel, mapped characteristics of vegetation inter-annual and intra-annual changes through trend analysis, and clustered the pixels with significant vegetation changes by the k-means method based on the vegetation types and change characteristics. After identifying vegetation change patterns and their driving factors, an elasticity method based on the Budyko hypothesis was applied to explore the hydrological responses to the different vegetation change patterns. Finally, we provided suggestions for integrated vegetation and water management in the YRB.

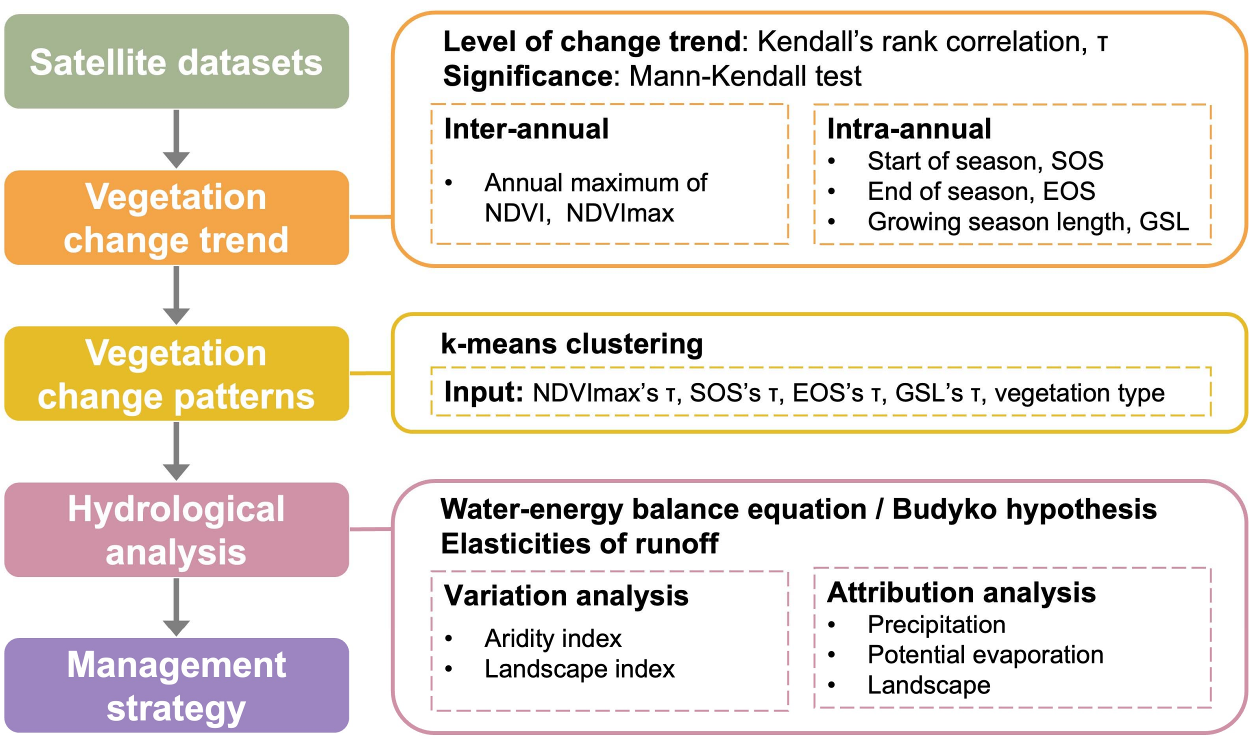

Figure 2 Framework for data analysis

2.2.1 Remote-sensing based vegetation phenology identification

We used the Savitzky-Golay filter to reconstruct remote sensing vegetation data and a double Logistic function to fit the data, and thus obtained the vegetation phenological characteristic values (Chen et al., 2004; Savitzky and Golay, 1964).

The equation of the Savitzky-Golay filter applied to the vegetation data is as follows:

$$NDVI_j^* = \frac{\sum_{i=-m}^{i=m} W_i \cdot NDVI_{j+i}}{N} \tag{1}$$

, where $NDVI_{j+i}$ is the $j+i$-th NDVI of the original data sequence, $NDVI_j^*$ is the j-th NDVI of the reconstructed data sequence, W_i is the weight of the i-th original data in the filter during a local fitting smoothing process, N indicates the number of data processed in a sliding window, m is half of the width of the sliding window, $N = 2m + 1$.

To obtain the surface phenology, the reconstructed NDVI sequence was fitted with the following double Logistic function (Beck et al., 2006; Fisher et al., 2006):

$$f(t) = v_1 + v_2\left(\frac{1}{1+e^{-m_1(t-n_1)}} - \frac{1}{1+e^{-m_2(t-n_2)}}\right) \tag{2}$$

, where $f(t)$ is the NDVI value at the Julian day t, v_1 is the background NDVI level for the whole year, and v_2 is the amplitude of NDVI for the whole year. The parameters m and n are used to determine the overall slope and basic phase of the NDVI increase phase and decrease phase, respectively; m_1, n_1 and m_2, n_2 are two pairs of the parameters. The six parameters of the model are solved by the Levenberg-Marquardt algorithm. The Julian day corresponding to the maximum slope of the fitted model curve is identified as the start-of-season (SOS), while the Julian day corresponding to the minimum slope is identified as the end-of-season (EOS). The growing season length (GSL) is then calculated as the difference between the SOS and EOS. Notably, this method is objective and does not rely on subjective experience, making it suitable for analyzing various types of vegetation (Figure 3).

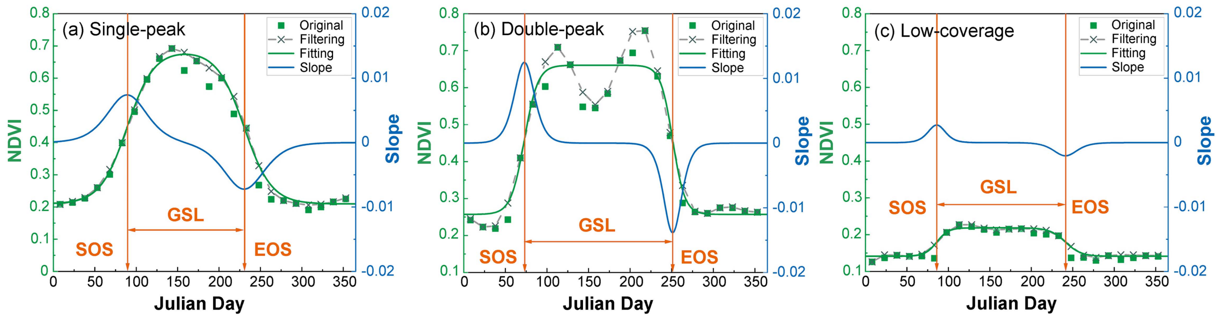

Figure 3 Examples of phenological indicators extraction. Extraction for a single-peak pixel (a), a double-peak pixel (b), and a pixel with low vegetation coverage (c).

2.2.2 Trend analysis and clustering

We chose the Kendall rank correlation coefficient τ to quantify the likelihood of the changing trend of the data sequence (Kendall, 1990). The value range of τ is in [-1, 1], where a positive τ indicates an increasing trend and a negative τ indicates a decreasing trend. The closer the absolute value to 1, the more significant the changing trend. To determine the significance of the trend, the Mann-Kendall nonparametric test method was employed (Kendall, 1990; Mann, 1945). A significance level of 0.05 was set to assess the trend.

To summarize the inter-annual and intra-annual variation characteristics of vegetation, we utilized the normalized vegetation information and Kendall's τ of the four vegetation characteristics (NDVImax, SOS, EOS, and GSL) as input for k-means clustering. Specifically, the vegetation of a pixel was considered to have significant changes when at least one of the four sequences passed the Mann-Kendall significance test. The k-means method was then applied to the dataset composed of the vegetation types and Kendall's τ of the four vegetation characteristics to cluster the pixels with significant vegetation changes (Arthur and Vassilvitskii, 2006).

2.2.3 Elasticity of runoff derived from the Choudhury–Yang equation

The long-term hydroclimatic characteristics of the watershed obey the principle of water and energy balance under certain climate and vegetation conditions (Budyko, 1974). The Choudhury-Yang equation is an empirical water-energy balance equation (Yang et al., 2008), expressed as:

$$E = \frac{PE_0}{(P^n + E_0^n)^{1/n}} \tag{3}$$

, where E is the mean annual actual evaporation, P is the mean annual precipitation, E_0 is the mean annual potential evaporation, and the parameter n represents the catchment landscape characteristics that are mainly related to properties of soil, topography, and vegetation.

From the long-term catchment water balance equation, $R = P - E$, where R is the mean annual runoff. Assuming P, E_0 and n are independent variables, the total differential of R can be written as:

$$dR = \frac{\partial f}{\partial P} dP + \frac{\partial f}{\partial E_0} dE_0 + \frac{\partial f}{\partial n} dn \tag{4}$$

Define the precipitation elasticity of runoff (ε_P) as $\varepsilon_P = \frac{dR/R}{dP/P}$, the potential evaporation elasticity of runoff (ε_{E_0}) as $\varepsilon_{E_0} = \frac{dR/R}{dE_0/E_0}$, and the catchment landscape elasticity of runoff (ε_n) as $\varepsilon_n = \frac{dR/R}{dn/n}$. Then Eq. (6) can be transformed into the following form (Xu et al., 2014):

$$\frac{dR}{R} = \varepsilon_P \frac{dP}{P} + \varepsilon_{E_0} \frac{dE_0}{E_0} + \varepsilon_n \frac{dn}{n} \tag{5}$$

, in which the elasticities of runoff are:

$$\varepsilon_P = \frac{(1+\emptyset^n)^{1+1/n} - \emptyset^{n+1}}{(1+\emptyset^n)[(1+\emptyset^n)^{1/n} - \emptyset]} \tag{6}$$

$$\varepsilon_{E_0} = \frac{1}{(1+\emptyset^n)[1-(1+\emptyset^{-n})^{1/n}]} \tag{7}$$

$$\varepsilon_n = \frac{ln\,(1+\emptyset^n) + \emptyset^n ln(1+\emptyset^{-n})}{n(1+\emptyset^n)[1-(1+\emptyset^{-n})^{1/n}]} \tag{8}$$

, where $\emptyset$ is the aridity index and $\emptyset = E_0/P$.

2.2.4 Attribution analysis

We divided the study period into two sub-periods. Here we set the breakpoint as 1999 because the Grain for Green project began this year. Period 1 is from 1950 to 1999 (P1) and period 2 is from 2000 to 2020 (P2). The mean annual runoff during period 1 was denoted as R1 and the mean annual runoff during period 2 was denoted as R2. The change of annual runoff from period 1 to period 2 can be written as:

$$\Delta R = R_2 - R_1 \tag{9}$$

This change of runoff (ΔR) is attributed to the impacts of climate variation and watershed landscape change. Assuming the landscape change is mainly induced by land use/cover change, the change of runoff can be written as:

$$\Delta R = \Delta R_c + \Delta R_l \tag{10}$$

, where ΔR_c is climate-induced runoff change, and ΔR_l is land cover-induced runoff change. Runoff change due to climate variation (ΔR_c) includes runoff change due to precipitation variation (ΔR_P) and potential evaporation variation (ΔR_{E_0}).

From Eq. (7), we can estimate the changes of runoff from P1 to P2 induced by variations of precipitation, potential evaporation, and land use/cover as:

$$\Delta R_P = \varepsilon_P \frac{R}{P} \Delta P,\ \Delta R_{E_0} = \varepsilon_{E_0} \frac{R}{E_0} \Delta E_0, \Delta R_l = \varepsilon_n \frac{R}{n} \Delta n \tag{11}$$

, where $\Delta P = P_2 - P_1$ and $\Delta E_0 = E_{0,2} - E_{0,1}$, representing a change in mean annual precipitation and potential evaporation from P1 to P2; $\Delta n = n_2 - n_1$, n_1, and n_2 represent landscape condition in P1 and P2, respectively. n_1 and n_2 can be estimated by solving Eq. (5) with mean annual P and E_0 for P1 and P2. Δn mainly indicates the changes in vegetation because the properties of soil and topography are relatively stable (Xu et al., 2014).

3 Data

We utilized NOAA CDR NDVI from 1982 to 2020 to detect changes in vegetation (Eric et al., 2018). This remote sensing product provides daily data with a spatial resolution of 0.05°×0.05. This remote sensing product provides daily data at a spatial resolution of 0.05° × 0.05°. The vegetation-type information was obtained from the basic maps of national natural resources and natural conditions, "Vegetation Atlas of China (1:1 000 000 000)" (Hou, 2001). We selected ERA5-Land from 1950 to 2020 for the series of total precipitation, total evaporation, and potential evaporation in hydrometeorological analysis. ERA5-Land is a reanalysis dataset with a spatial resolution of 0.1° × 0.1°, providing a consistent view of the evolution of land variables (Muñoz-Sabater et al., 2021). The temporal and spatial resolution of ERA5-Land makes this dataset useful for various land surface applications, such as flood or drought forecasting (Grigorev et al., 2022; Kageyama and Sawada, 2022).

4 Results

4.1 Vegetation change patterns

Through a remote-sensing-based vegetation phenology identification process, we obtained the annual start-of-season (SOS), end-of-season (EOS), and growing season length (GSL) of vegetation in the YRB. We then calculated the Kendall rank correlation coefficient τ of the four vegetation indicators (NDVImax, SOS, EOS, and GSL) on a pixel-by-pixel basis from 1982 to 2020 in the YRB and created a map of the temporal and spatial trends of vegetation indicators (Figure 4). From 1982 to 2020, NDVImax showed an upward trend in almost the entire YRB, with significant improvements in vegetation observed in the northeastern part of S1 and S2, irrigated areas in S3, and arid and semi-arid areas of the central Loess Plateau in S4-S6 (Figure 4 a).

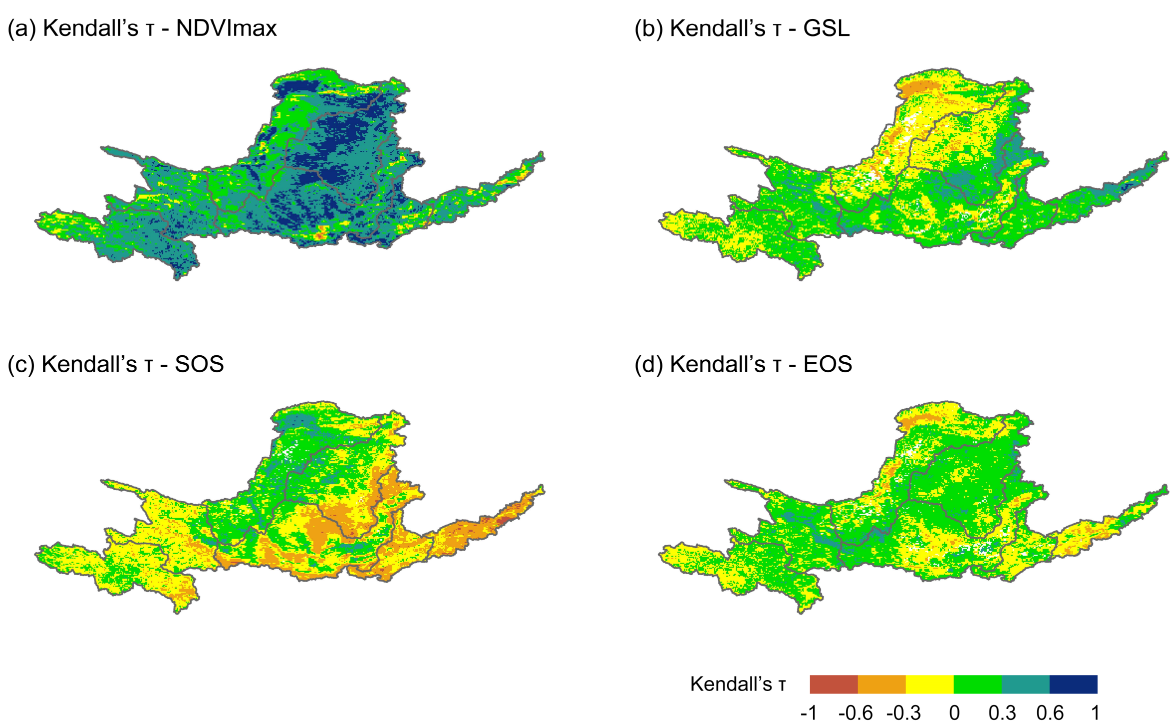

Figure 4 Temporal and spatial trend of vegetation indicators in the Yellow River Basin (1982-2020). Kendall’s τ of the annual maximum (NDVImax) (a), start-of-season (SOS) (b), end-of-season (EOS) (c), and growing season length (GSL) (d) from 1982 to 2020.

The mean τ of NDVImax in S1-S3 was above 0.3, the mean τ in S5 and S6 was above 0.4, and the mean τ in S4 even reached 0.55. The central part of the Loess Plateau, which coincided with the main revegetation implementation areas, showed the most significant improvement in vegetation. Changes in phenological indicators were relatively strong in irrigation and humid areas (Figure 4 b-d). The upstream irrigation areas in S3 showed a trend of delayed SOS, advanced EOS, and shortened GSL, while the downstream irrigation areas in S6 and S7 showed a trend of advanced SOS and extended GSL. Humid and semi-humid areas dominated by forests and shrubs demonstrated an advance in SOS and an extension of GSL. Among SOS, EOS, and GSL, the SOS of vegetation in the YRB showed the most significant changes.

The results of vegetation change clustering in the YRB are shown in Figure 5. After enumeration, the optimal number of clusters was determined to be k = 7, indicating seven distinct patterns of vegetation change. When compared to k = 6, the majority of pixels in the newly identified group were located in the source region (blue area in Figure 5 a), characterized by its high altitude and minimal human disturbance, which was markedly different from other areas in the YRB. On increasing k to 8, the pixels in the new group were found to be scattered with a small count number (red area in Figure 5 c). Based on the clustering analysis results, Figure 5 (a) presents the spatial distribution of the seven identified patterns of vegetation change in the YRB, while Table 2 summarizes the key characteristics of these seven clusters.

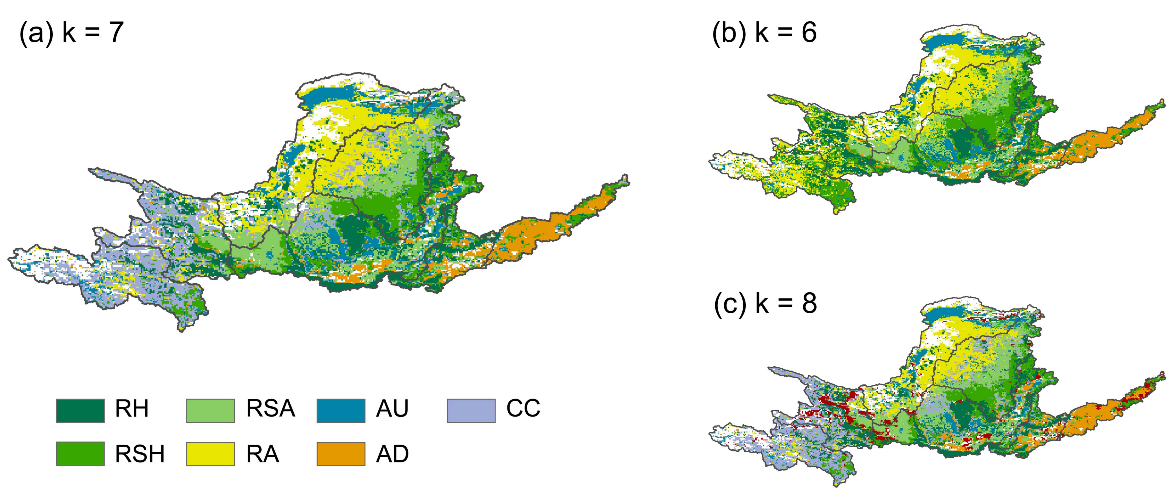

Figure 5 Results of vegetation change clustering in the Yellow River Basin. Number of cluster k =7(a), k=6 (b), and k=8 (c). RH is for Revegetation - Humid Area; RSH is for Revegetation - Semi-Humid area; RSA is for Revegetation - Semi-Aumid area; RA is for Revegetation - Semi-Arid area; AU is for Agricultural alteration – Upstream (AU); AD is for Agricultural alteration – Downstream (AU); CC is for Climate Change.

Table 2 Vegetation change patterns in the Yellow River Basin

Clusters	NDVI max-τ	SOS-τ	EOS-τ	GSL- τ	Vegetation types in the 1980s	Drivers
RH	0.48	-0.29	0.07	0.22	shrublands (27.3%), broadleaf forests (26.0%), needleleaf forests (17.3%)	Revegetation - humid area (RH)
RSH	0.52	-0.35	0.13	0.29	croplands (65.3%), meadows (10.6%), herbosa (9.4%)	Revegetation - semi-humid area (RSH)
RSA	0.46	0.06	0.15	0.06	croplands (86.8%), grasslands (9.4%), meadows (1.3%)	Revegetation - semi-arid area (RSA)
RA	0.47	0.20	0.07	-0.15	grasslands (62.2%), deserts (12.3%), meadows (11.6%)	Revegetation - arid area (RA)
AU	0.55	0.13	-0.18	-0.19	croplands (64.7%), meadows (17.7%), grasslands (7.4%)	Agricultural alteration – Upstream (AU)
AD	0.15	-0.36	-0.09	0.22	croplands (89.8%), herbosa (2.4%), meadows (2.0%)	Agricultural alteration – Downstream (AD)
CC	0.42	-0.11	0.08	0.11	meadows (42.6%), grasslands (29.0%), shrublands (11.9%)	Climate change (CC)

The four clusters identified as Revegetation - Humid area (RH), Revegetation - Semi-Humid area (RSH), Revegetation - Semi-Arid area (RSA), and Revegetation - Arid area (RA) were all driven by revegetation. These clusters were primarily distributed in the Loess Plateau region with notable improvements in vegetation conditions, as evidenced by the increased NDVImax ($\tau > 0.4$). The feedback of revegetation on different hydrothermal conditions was manifested in distinct vegetation phenology patterns. The revegetation clusters were generally banded and distributed with increasing drought levels from southeast to northwest.

RH was primarily distributed in S5, characterized by humid areas with relatively good vegetation conditions even before revegetation. The phenological characteristics of RH were advanced SOS ($\tau = -0.29$), delayed EOS ($\tau = 0.07$), and extended GSL ($\tau = 0.22$). RSH was mainly concentrated in S4 and S5, semi-humid areas dominated by croplands (65.3%), reflecting the change pattern driven by the Green for Grain projects in semi-humid areas. The phenological changes of RSH were similar to that of RH but with stronger trends. RSA was primarily concentrated in S4 and S5, semi-arid areas with 86.8% of croplands, reflecting the vegetation change patterns in semi-arid areas driven by the Green for Grain projects. In RSA, the SOS was slightly delayed (τ = 0.06), the GSL was weakly extended (τ = 0.06), but the delay trend of EOS was the strongest among the four clusters driven by revegetation (τ = 0.15). RA was mainly concentrated in S3 and S4, arid areas, reflecting the change pattern driven by ecological engineering to control desertification in arid areas. The phenological changes of RA included delayed SOS (τ = 0.20) and significantly shortened GSL (τ = -0.15). The vegetation conditions in the arid area were extremely poor, and before ecological projects such as desertification control, the NDVI sequences were flat, had no obvious peak, and the identified GSL was long (see Figure 3 c). The restored sandy vegetation had a short growing season, as indicated by a small peak in the NDVI sequences.

Both agricultural planting structure alteration upstream (AU) and agricultural intensification downstream (AD) were predominantly observed in irrigation areas where vegetation change patterns were driven by agricultural practices. AU was primarily observed in S3, the upstream irrigation area represented by the Hetao region. NDVImax significantly increased (τ = 0.55) in AU, while the start of season (SOS) was delayed, the end of season (EOS) was advanced, and the growing season length (GSL) was shortened. In contrast, AD was mainly observed in S7, the downstream irrigation areas of the Yellow River Basin (YRB). The NDVImax increase in AD was the smallest among the seven groups (τ = 0.15), but SOS significantly advanced (τ = -0.36). Diverse agricultural practices caused different vegetation feedback in AU and AD.

In AU, to reduce water consumption, the area under wheat cultivation shrank rapidly, and sunflowers and corn were planted instead of wheat. For sunflowers, the GSL is 90-130 days, and SOS is in mid-July to mid-August; the GSL of corn is 90-100 days, and SOS is in mid-to-late July. In contrast, the GSL is 100-130 days, and the SOS is in early April for wheat. The shorter GSL of sunflowers and corn and the later SOS led to the phenological changes in AU, with delayed SOS, advanced EOS, and shortened GSL. AD was primarily situated in the downstream irrigation areas, which are the main grain-producing regions in China. In contrast to AU, AD maintained the planting pattern of winter wheat and summer corn. With the modernization and intensification of agriculture, grain yield in AD grew rapidly. For instance, the irrigated area in Henan (a province in lower YRB) increased from 3.3 million ha to 5.6 million ha, the total power of agricultural machinery increased from 13.6 million kW to 104.6 million kW, and the total grain output increased from 22.2 million tons to 68.3 million tons from 1980 to 2020. The large-scale planting of winter wheat and summer corn resulted in a prominent double-peak NDVI curve, with significant advances in SOS and extensions in GSL in AD.

Climate change (CC) predominantly affected S1 and S2, which had fewer anthropogenic stressors. The significant warming of the Qinghai-Tibet Plateau led to an improvement in vegetation coverage, an advance in the SOS, a delay in the EOS, and an extension of the GSL. Nonetheless, the vegetation changes triggered by climate changes were generally less pronounced when compared to those resulting from human activities.

4.2 Hydrometeorological changes based on the Budyko hypothesis

We analyzed the hydrological responses to different vegetation changes using the Choudhury-Yang equation based on the Budyko hypothesis. Figure 6 presents the annual mean aridity factor (E_0/P , $\emptyset$), actual evaporation factor (E/P), and landscape factor (n), and their differences during two time periods, 1950-1999 (P1) and 2000-2020 (P2). The YRB experienced significant changes in E_0/P, E/P, and n. E_0/P increased from the southeast to the northwest in all sections except S1. Between P1 and P2, E_0/P decreased in S1 but increased in the other six sections. Notably, high $\Delta E_0/P$ (> 1.0) was primarily observed in S3, S5, and S7, which are mainly distributed in the upstream and downstream irrigation areas. This suggests that agricultural activities may aggravate the trend of local aridification in the YRB. The distribution of the $\Delta E/P$ between P1 and P2 is different from E_0/P. E/P decreased slightly in S1 and increased significantly in the humid and semi-humid areas in S4 and S5. Moreover, the map of n obtained by solving the Choudhury–Yang equation revealed that n was relatively low in high altitude S1, whereas it was relatively high in the arid area in S3 and S4, and the humid area in S5 and S6. From P1 to P2, Δn exhibited a substantial increase in S4-S6, while it decreased considerably in S1-S3. The index n determines the overall shape characteristics of the Budyko curve, and is influenced by local vegetation, topography, and soil. Higher n under the same aridity condition (E_0/P) indicates that the local landscape is more efficient in utilizing precipitation for evaporation. This increased efficiency can be attributed to vegetation growth since the features of topography and soil are relatively stable over time.

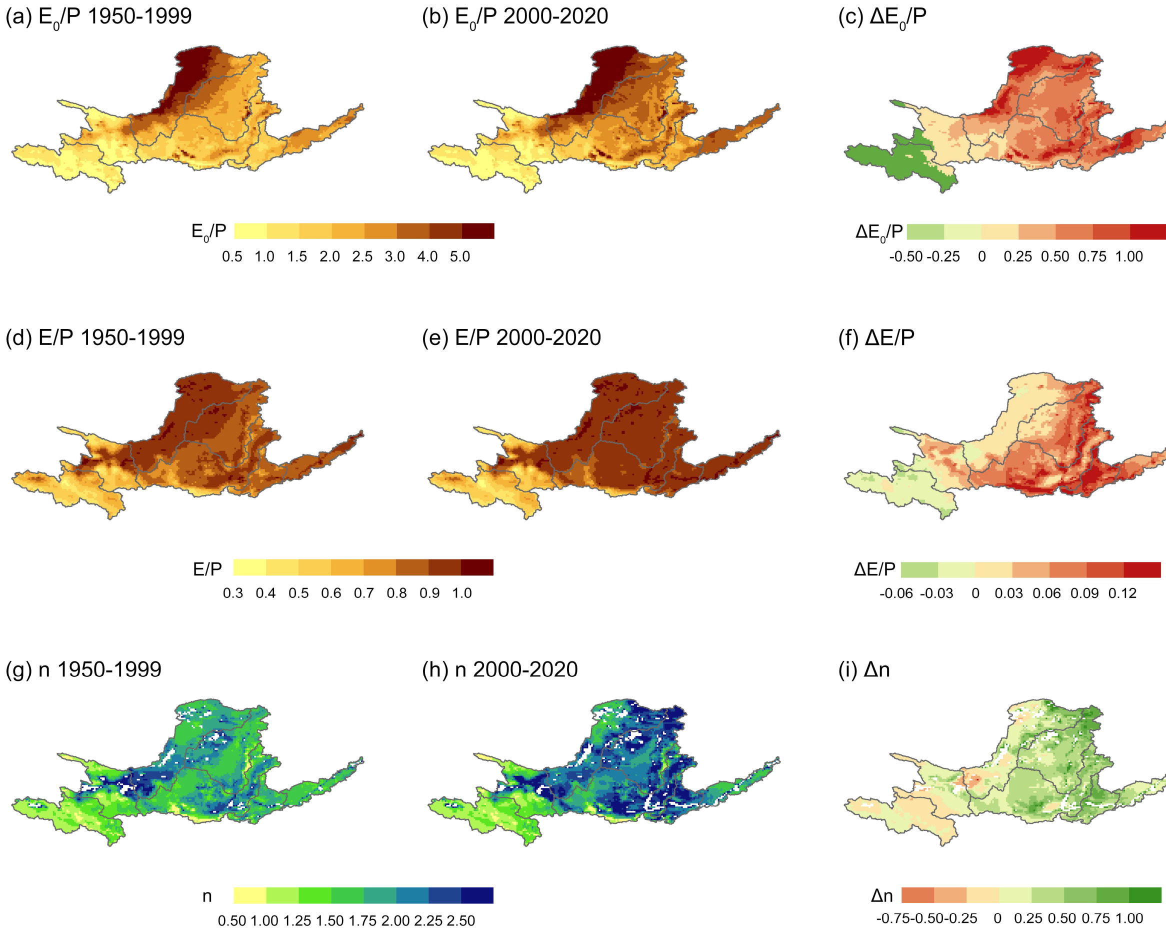

Figure 6 Map of hydrometeorological indicators and their differences in the two periods. E_0/P (a), E/P (d), n (g) in 1950-1999; E_0/P (b), E/P (e), and n (h) in 2000-2020; the difference values of E_0/P (c), E/P (f), and n (i) between the two periods. E_0/P is the ratio of potential evaporation to precipitation; E/P is the ratio of actual evaporation to precipitation; n is the landscape factor by solving Choudhury–Yang equation.

Figure 7 presents the annual mean values of E_0/P and E/P in the seven sections and the seven clusters of vegetation change patterns for the two periods. The zonal mean differences between P1 and P2 for $\Delta E_0/P$, $\Delta E/P$, and Δn, are provided in Table 3. The analysis based on the seven sections helps clarify the spatial distribution patterns, while the analysis based on the clustering benefits the understanding of the impacts of the different vegetation change patterns. Among the seven sections, S1 had the smallest change and showed a humidification trend ($\Delta E_0/P = -0.04$). The aridity factor E_0/P increased the most in S3 ($\Delta E_0/P = 0.79$), followed by S7 ($\Delta E_0/P = 0.72$). The landscape factor n increased the most in S4, S5, and S6, with Δn being 0.48, 0.39, and 0.58, respectively. Among the seven clusters, the aridity increment of the cluster driven by climate change (CC) was the lowest ($\Delta E_0/P = 0.18$), and so was the improvement in landscape related to vegetation changes ($\Delta n = 0.12$). The aridity increment was the highest in the agriculture-driven AU ($\Delta E_0/P = 0.77$), followed by that in AD ($\Delta E_0/P = 0.67$). As for the four revegetation-driven groups, RA had the most significant aridification trend ($\Delta E_0/P = 0.60$). The mean Δn of RSH was 0.40, and the mean Δn of RSA was 0.39, larger than the other five clusters. The humid region of the YRB had larger vegetation coverage initially, and hence, had limited potential for improvement in n compared to the semi-arid and semi-humid transitional zones. Similarly, the arid area had a lower potential for n increment due to water and heat constraints. In addition to the fact that revegetation may lead to increased drought risk, it is important to note that AU and AD have a significant increase in both ($\Delta E_0/P = 0.77$ and n. The drastic changes in these two clusters highlight the need to focus on agricultural water use while managing vegetation and water resources in the YRB.

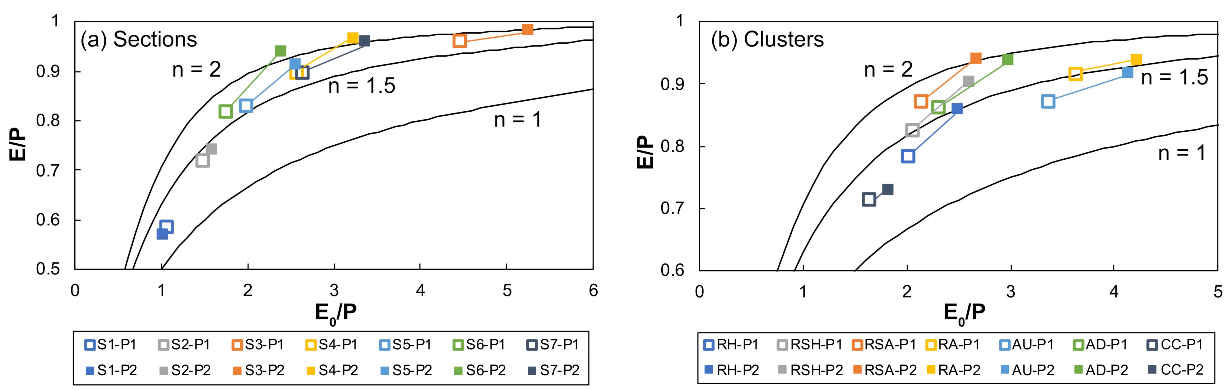

Figure 7 Budyko curves for the seven sections (a) and the seven clusters (b). P1 is for the period 1 1950-1999; P2 is for the period 2000-2020. S1-S7 are the 7 sections based on the division of the Yellow River; RH is for Revegetation - Humid Area; RSH is for Revegetation - Semi-Humid area; RSA is for Revegetation - Semi-Humid area; RA is for Revegetation - Semi-Arid area; AU is for Agricultural alteration – Upstream (AU); AD is for Agricultural alteration – Downstream (AU); CC is for Climate Change.

Table 3 Zonal statistic of hydrometeorological indicators variation in the seven sections and the seven clusters

Section	ΔE/P	$\Delta E_0/P$	Δn	Cluster	ΔE/P	$\Delta E_0/P$	Δn
S1	-0.02	-0.04	-0.02	RH	0.07	0.49	0.30
S2	0.02	0.10	0.07	RSH	0.08	0.55	0.40
S3	0.02	0.79	0.23	RSA	0.07	0.53	0.39
S4	0.07	0.66	0.48	RA	0.02	0.60	0.24
S5	0.08	0.57	0.39	AU	0.04	0.77	0.36
S6	0.12	0.65	0.58	AD	0.07	0.67	0.36
S7	0.06	0.72	0.29	CC	0.02	0.18	0.12

4.3 Vegetation's influence on runoff change

We evaluated the impact of various vegetation change patterns on runoff by utilizing an elasticity method based on the Choudhury-Yang equation. Figure 8 displays the distributions of precipitation elasticity of runoff (ε_P), potential evaporation elasticity of runoff (ε_{E_0}), and landscape elasticity of runoff (ε_n). The spatial distribution patterns of ε_P and ε_{E_0} were similar, with relatively large absolute values observed in both arid and humid regions. The distribution pattern of ε_n was comparable to that of aridity shown in Figure 6, with small absolute values in the source area and gradually increasing from southeast to northwest.

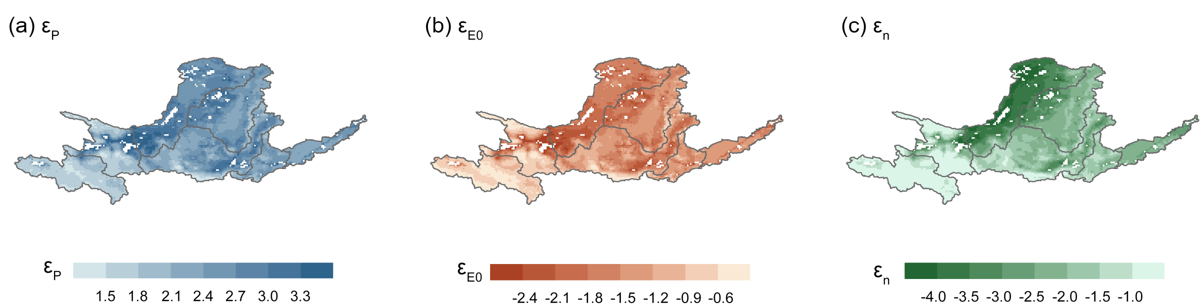

Figure 8 Elasticity of runoff related to (a) precipitation, (b) potential evaporation, and (c) landscape index n.

Figure 9 displays the daily runoff depth differences (ΔR) between P1 and P2 induced by the changes in precipitation, potential evaporation, and landscapes. The mean ΔR values in the seven sections and the seven clusters were presented in Figure 10. Among the seven sections (Figure 10 a), only S1 experienced an increase in runoff, which is mainly due to precipitation changes. The ΔR_P in S1 is 0.07mm, and the contribution rate of precipitation reached 95.5%, consistent with prior research on increasing runoff trend in the Yellow River source region caused by warming and humidification of the Qinghai-Tibet Plateau (Wang et al., 2018). S2 was the only section where evaporation had the most significant impact on changes in runoff, with a total ΔR of approximately 0.05mm, of which ΔR_{E_0} accounted for 47.8%, and ΔR_n accounted for 35.3%. The total ΔR in S3-S6 increased successively and was positively related to local humidity, indicating that precipitation changes had a more substantial impact on runoff reduction in wetter regions.

According to the mean values of seven clusters (Figure 10 b), ΔR_P of the climate-driven cluster CC was 0.09 mm, indicating that precipitation changes led to an increase in runoff. We observed a slight reduction in runoff due to potential evaporation, with mean absolute ΔR_{E_0} in all seven groups less than 0.05 mm. Conversely, vegetation changes caused a significant decline in the runoff. The ΔR_n of the four clusters under revegetation, RH, RSH, RSA, and RA, were -0.12, -0.13, -0.11, and -0.03 mm, respectively. Notably, in the two clusters under agricultural alteration patterns, the ΔR_n was -0.08 mm in AU and -0.12 mm in AD, approaching that caused by vegetation restoration. In contrast, the ΔR_n of CC was -0.04 mm. Among the six human activity-driven clusters, precipitation contributed 20.3% to 41.8% to runoff variation, while landscape changes contributed 44.1% to 60.7%.

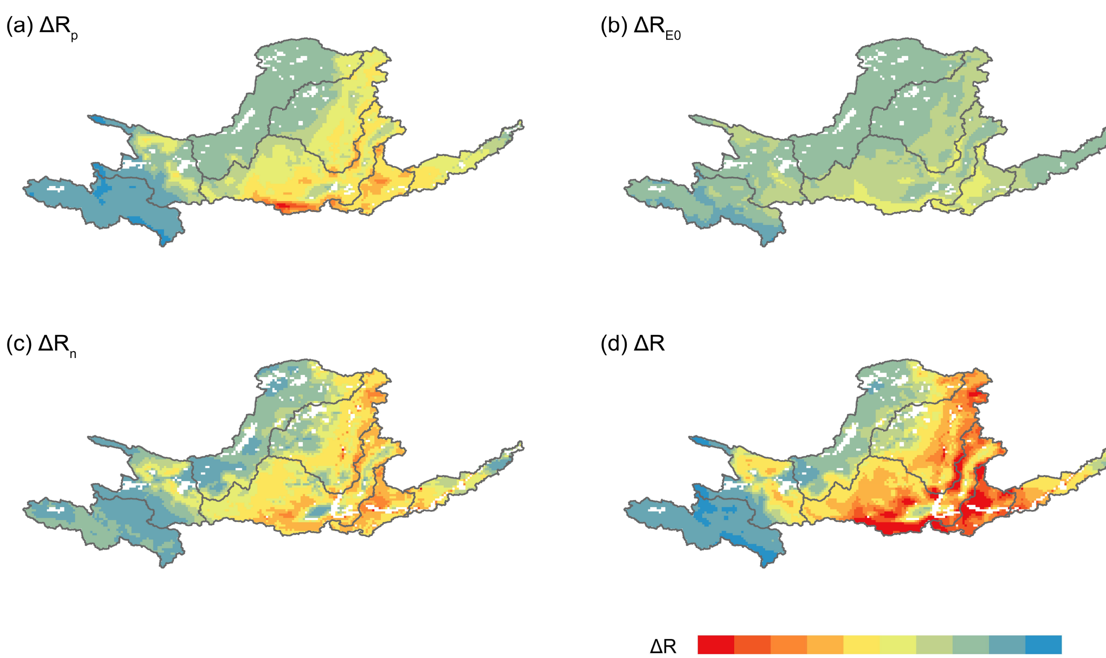

Figure 9 Changes of daily runoff depth caused by changes in precipitation (a), potential evaporation (b), landscape index n (c), and total runoff depth change (d) from 1950-1999 to 2000-2020.

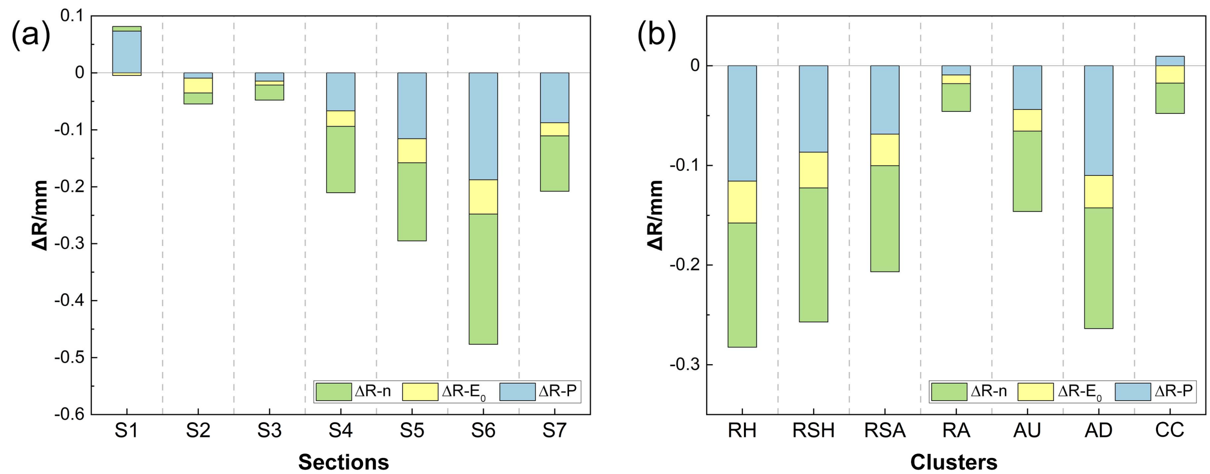

Figure 10 Runoff depth changes in (a) the seven sections and (b) the seven clusters. S1-S7 are the 7 sections based on the division of the Yellow River; RH is for Revegetation - Humid Area; RSH is for Revegetation - Semi-Humid area; RSA is for Revegetation - Semi-Aumid area; RA is for Revegetation - Semi-Arid area; AU is for Agricultural alteration – Upstream (AU); AD is for Agricultural alteration – Downstream (AU); CC is for Climate Change.

5 Discussion

5.1 Agricultural vulnerability in YRB

According to our analysis, the Yellow River Basin (YRB) is facing a severe water shortage, which is further exacerbated by the emergence of a significant drought trend. The upstream and downstream irrigation areas (in S3 and S7) exhibited the most notable drought trend in the YRB, which represents a threat to both water and food security. Our findings emphasize the crucial role of agriculture in the water-food-ecology conflicts that persist in the YRB. Our analysis indicates that agricultural activities are a major contributor to severe water depletion, similar to the greening driven by ecological engineering as reported by many researchers.

The impact of agricultural change on runoff, as quantified as ΔR_n in the two clusters under agricultural alteration patterns AU and AD, is close to that in the revegetation clusters. Despite the focus on agricultural water conservation since the 1990s, the actual effect appears to be weak. In the downstream irrigation area, agricultural mechanization and expansion of the wheat planting area led to increased agricultural water use. Conversely, agricultural water consumption had decreased substantially in the upstream irrigation area through the development of water-saving irrigation technologies and changes in planting crops. However, the mean groundwater depth still dropped rapidly in the upstream irrigation area. One of the reasons for this is that the desert oasis requires water to sustain groundwater levels, and the irrigation water considered as waste is necessary to maintain the oasis's ecological functions. In other words, elevating irrigation efficiency in arid areas could be harmful.

Furthermore, the agricultural vulnerability in the YRB tends to increase with the combined effect of climate change and ecological projects, which lead to decreasing precipitation and increasing evaporation from improved vegetation. Although the climate of AU and AD varied greatly, the aridity factor increments between P1 and P2 ($\Delta\, E_0/P$) in the two agricultural clusters reached 0.77 and 0.67, respectively, which are larger than that of any other cluster. The decreasing precipitation and increasing evaporation contributed significantly to runoff reduction in both AU and AD, increasing the likelihood of drought in the YRB. In the central plain around Henan, China's principal crop-production area in YRB, 1.05 million hectares were damaged by drought in 2022, (https://www.henan.gov.cn/2022/08-24/2566944.html; in Chinese). Water demand also increased rapidly with ecological engineering and socioeconomic development in the YRB. Given the increasing frequency of extreme weather events and the close relationship between grain yields in the YRB and national food security, it is imperative to prepare for an uncertain future.

5.2 Measures to alleviate water-food-ecology conflicts in the YRB

The water-food-ecology conflicts directly challenge the sustainable development goals including Target 2 (Zero Hunger), 6 (Clean Water and Sanitation), and 15 (Life on Land) (Zhou et al., 2023). With the increasing aridification trend in the YRB and growing water demand, those conflicts will be exacerbated further. Consequently, there is an urgent need for comprehensive strategies that balance the trade of development and ecological protection. Given that agriculture is the largest water use sector in the YRB, improving the efficiency of agricultural water use is undoubtedly necessary. However, excessive water conservation in arid areas can lead to local drought, and elevating agricultural water efficiency in the upstream regions to levels comparable to those in humid downstream regions is challenging.

In addition to advances in agricultural technologies, replacing high-water-consuming crops such as wheat with low-water-consuming alternatives like potatoes and beans is a feasible way to reduce water consumption, particularly in downstream croplands. It is worth noting that ecological greening projects can significantly increase evaporation, and in such severe water shortage, optimizing current tree species in revegetation areas, such as replacing trees with shrubs for less evaporation in semi-arid or semi-humid areas, could prove effective in alleviating the conflicts. Another strategy that can help reduce water scarcity in the YRB is using water from outside the river basins through water diversion projects instead of relying solely on local freshwater resources. Accelerating the operation of the west route of the South Water to North Project to release the water pressure in the upper reaches of the YRB could be a meaningful step in this direction.

5.3 Comparison with previous work

Diverse hydrological methods and models have been employed to investigate the dramatic hydrological changes in the YRB. Our study differs from previous research in two main aspects: first, we identified the patterns of vegetation changes and, second, we conducted a distributed attribution analysis of runoff changes based on the Budyko hypothesis. Vegetation was selected as the key indicator in this study as it provides crucial feedback on environmental changes in the YRB. Through clustering the inter-annual and intra-annual characteristics of vegetation changes, we identified seven distinct vegetation change patterns and corresponding distributions.

Compared to the simple basin division based on the upstream-downstream relationship, clustering resulted in lower heterogeneity within the pixel clusters, which facilitated the analysis of hydrometeorological responses to various driving factors of vegetation change. By incorporating phenology-represented vegetation intra-annual characteristics, we analyzed vegetation changes in both croplands and revegetation areas under the same framework. While previous research has focused on the impact of vegetation changes in revegetation areas on the

Loess Plateau, where vegetation shows significant inter-annual changes due to increasing coverage (Chen et al., 2015; Feng et al., 2016), our study demonstrates that agricultural activities also have a significant impact on the hydrology of the YRB, even though the change in vegetation coverage due to agriculture is relatively weak. Given the increasing threats from climate change and growing ecological water demand, it is crucial to pay attention to agriculture in the water-food-ecology conflicts of the YRB.

Another novel aspect of our study is the use of the gridded reanalysis product ERA5-Land to perform gridded runoff change attribution analysis at the scale of the entire YRB. By replacing site observation data with ERA5-Land, we performed a distributed hydrological analysis based on the Budyko hypothesis, in which the runoff changes on every pixel with the size of 0.1°×0.1° was calculated. With the advantage of earth model foundation, the results have good continuity and effectively presented the spatial differentiation in the YRB. The distributed runoff change analysis supports the investigation of the hydrological responses of the scattered seven vegetation change clusters. In contrast to previous studies that typically focused on small sub-basins of the YRB due to the limits of site data, our results are consistent with the site-data-based analysis in the distribution and value range of aridity, landscape parameter n, elasticities, and runoff changes (Li et al., 2019). Furthermore, this method requires fewer data and is easier to apply than complicated process-based physical models, making it more suitable for large-scale basin analysis.

6 Conclusions

To address the challenging water-food-ecology conflicts in the YRB, we developed an analysis framework based on vegetation change and the Budyko hypothesis. (a) Seven vegetation change patterns were identified based on inter-annual and intra-annual vegetation changes: four are driven by revegetation activities, presenting the different feedbacks of revegetation projects in humid, semi-humid, semi-arid, and arid areas; two are driven by agricultural alteration which are the planting structure changes represented by the upstream Hetao irrigation area and agricultural mechanization represented by the downstream North Plain irrigation area; the last one is driven by climate changes and mainly distributed in the source region. (b) The landscape index n increased most in the semi-humid and semi-arid areas under revegetation, while the aridity increased most in the upstream and downstream irrigation areas.

(c) Human-driven vegetation changes contributed to 44.1%–60.7% of local runoff reduction according to the attribution analysis based on the Budyko hypothesis. Specifically, the daily runoff depth reduction caused by agricultural changes is 0.08 mm upstream and 0.12 mm downstream, equivalent to 29-44 mm on an annual scale, approaching that caused by vegetation restoration. (d) Agriculture tended to be more vulnerable due to the combined effect of climate change and greening driven by ecological engineering. To alleviate water-food-ecology conflicts, we have to pay attention to food security and be prepared for the future with increasing drought risk.

Acknowledgments

M. Z. Xu acknowledges support from the National Natural Science Foundation of China (NSFC) (No. U2243222), and the Second Tibetan Plateau Scientific Expedition and Research Program (STEP) (No. 2019QZKK0903). G. Penny acknowledges support from the Singapore Ministry of Education Academic Research Fund Tier 1.

Open Research

The daily NDVI data used for vegetation variation analysis in the study are available at https://www.ncei.noaa.gov/data/land-normalized-difference-vegetation-index/access/ (AVHRR: doi:10.7289/V5ZG6QH9 / VIIRS: doi:10.25921/gakh-st76). The ERA5-land climate data used for hydrometeorological analysis in the study are available at https://cds.climate.copernicus.eu/cdsapp#!/dataset/reanalysis-era5-land-monthly-means?tab=form (DOI: 10.24381/cds.68d2bb30); The raster file of vegetation type in the 1980s, "Vegetation Atlas of China (1:1 000 000 000)", is available at https://www.resdc.cn/data.aspx?DATAID=122&WebShieldDRSessionVerify=0btkEkarZfy5FP

was3nm. All results and figures in this paper can be reproduced from the equations and parameters herein.

References

Arthur, D., and Vassilvitskii, S. (2006), k-means++: The advantages of careful seeding, Stanford.

Beck, P. S. A., Atzberger, C., Høgda, K. A., Johansen, B., and Skidmore, A. K. (2006), Improved monitoring of vegetation dynamics at very high latitudes: A new method using MODIS NDVI, *Remote Sensing of Environment*, *100*(3), 321-334. https://doi.org/10.1016/j.rse.2005.10.021

Best, J. (2018), Anthropogenic stresses on the world's big rivers, *Nature Geoscience*, *12*(1), 7-21. https://doi.org/10.1038/s41561-018-0262-x

Budyko, M. I. (1974), *Climate and life*, Academic press.

Chen, J., Jönsson, P., Tamura, M., Gu, Z., Matsushita, B., and Eklundh, L. (2004), A simple method for reconstructing a high-quality NDVI time-series data set based on the Savitzky–Golay filter, *Remote Sensing of Environment*, *91*(3-4), 332-344. https://doi.org/10.1016/j.rse.2004.03.014

Chen, Y., Wang, K., Lin, Y., Shi, W., Song, Y., and He, X. (2015), Balancing green and grain trade, *Nature Geoscience*, *8*(10), 739-741. https://doi.org/10.1038/ngeo2544

Eric, V., Chris, J., Ivan, C., Jeff, E., Ranga, M., Frederic, B., Ed, M., Robert, W., Martin, C., and Program, N. C. (2018), NOAA Climate Data Record (CDR) of Normalized Difference Vegetation Index (NDVI), Version 5., edited by N. N. C. f. E. Information.

Feng, X., et al. (2016), Revegetation in China's Loess Plateau is approaching sustainable water resource limits, *Nature Climate Change*, *6*(11), 1019-1022. https://doi.org/10.1038/nclimate3092

Fisher, J., Mustard, J., and Vadeboncoeur, M. (2006), Green leaf phenology at Landsat resolution: Scaling from the field to the satellite, *Remote Sensing of Environment*, *100*(2), 265-279. https://doi.org/10.1016/j.rse.2005.10.022

Gao, P., Li, P., Zhao, B., Xu, R., Zhao, G., Sun, W., and Mu, X. (2017), Use of double mass curves in hydrologic benefit evaluations, *Hydrological Processes*, *31*(26), 4639-4646. https://doi.org/10.1002/hyp.11377

Gao, Z., Zhang, L., Zhang, X., Cheng, L., Potter, N., Cowan, T., and Cai, W. (2016), Long-term streamflow trends in the middle reaches of the Yellow River Basin: detecting drivers of change, *Hydrological Processes*, *30*(9), 1315-1329. https://doi.org/10.1002/hyp.10704

Gerten, D., Schaphoff, S., Haberlandt, U., Lucht, W., and Sitch, S. (2004), Terrestrial vegetation and water balance—hydrological evaluation of a dynamic global vegetation model, *Journal of Hydrology*, *286*(1-4), 249-270. https://doi.org/10.1016/j.jhydrol.2003.09.029

Grigorev, V. Y., Kharlamov, M. A., Semenova, N. K., Sazonov, A. A., and Chalov, S. R. (2022), Impact of precipitation and evaporation change on flood runoff over Lake Baikal catchment, *Environmental Earth Sciences*, *82*(1), 16. https://doi.org/10.1007/s12665-022-10679-0

Hou, X. (2001). Vegetation Atlas of China (1:1 000 000 000). Beijing: Science Press. (in Chinese)

Kageyama, Y., and Sawada, Y. (2022), Global assessment of subnational drought impact based on the Geocoded Disasters dataset and land reanalysis, *Hydrol. Earth Syst. Sci.*, *26*(18), 4707-4720. https://doi.org/10.5194/hess-26-4707-2022

Karabulut, A., et al. (2016), Mapping water provisioning services to support the ecosystem–water–food–energy nexus in the Danube river basin, *Ecosystem Services*, *17*, 278-292. https://doi.org/10.1016/j.ecoser.2015.08.002

Kendall, M. G. (1990), *Rank correlation methods*, Oxford University Press, New York.

Kong, D., Miao, C., Wu, J., and Duan, Q. (2016), Impact assessment of climate change and human activities on net runoff in the Yellow River Basin from 1951 to 2012, *Ecological Engineering*, *91*, 566-573. https://doi.org/10.1016/j.ecoleng.2016.02.023

Li, Y., Liu, C., Yu, W., Tian, D., and Bai, P. (2019), Response of streamflow to environmental changes: A Budyko-type analysis based on 144 river basins over China, *Sci Total Environ*, *664*, 824-833. https://doi.org/10.1016/j.scitotenv.2019.02.011

Liu, J., Zhou, Z., Yan, Z., Gong, J., Jia, Y., Xu, C.-Y., and Wang, H. (2019), A new approach to separating the impacts of climate change and multiple human activities on water cycle processes based on a distributed hydrological model, *Journal of Hydrology*, *578*. https://doi.org/10.1016/j.jhydrol.2019.124096

Lu, B., Lei, H., Yang, D., and Fu, X. (2020), Separating the effects of revegetation and sediment-trapping dams construction on runoff and its application to a semi-arid watershed of the Loess Plateau, *Ecological Engineering*, *158*. https://doi.org/10.1016/j.ecoleng.2020.106043

Mann, H. B. (1945), Nonparametric tests against trend, *Econometrica: Journal of the econometric society*, 245-259.

Muñoz-Sabater, J., et al. (2021), ERA5-Land: a state-of-the-art global reanalysis dataset for land applications, *Earth System Science Data*, *13*(9), 4349-4383. https://doi.org/10.5194/essd-13-4349-2021

Pan, Y., et al. (2011), A Large and Persistent Carbon Sink in the World's Forests, *Science*, *333*(6045), 988-993. https://doi.org/10.1126/science.1201609

Ren, M. (2006), Sediment Discharge of the Yellow River, China: Past, Present and Future - A Synthesis. *Advances in Earth Science*, 2006(06): 551-563. (in Chinese)

Root, T. L., Price, J. T., Hall, K. R., Schneider, S. H., Rosenzweig, C., and Pounds, J. A. (2003), Fingerprints of global warming on wild animals and plants, *Nature*, *421*(6918), 57-60. https://doi.org/10.1038/nature01333

Savitzky, A., and Golay, M. J. (1964), Smoothing and differentiation of data by simplified least squares procedures, *Analytical chemistry*, *36*(8), 1627-1639.

The State Council of the People's Republic of China (2021), Planning outline for ecological conservation and high-quality development of the Yellow River Basin [Government Document]. http://www.gov.cn/zhengce/2021-10/08/content_5641438.htm. (in Chinese)

Wang, S., Fu, B., Piao, S., Lü, Y., Ciais, P., Feng, X., and Wang, Y. (2015), Reduced sediment transport in the Yellow River due to anthropogenic changes, *Nature Geoscience*, *9*(1), 38-41. https://doi.org/10.1038/ngeo2602

Wang, T., Yang, H., Yang, D., Qin, Y., and Wang, Y. (2018), Quantifying the streamflow response to frozen ground degradation in the source region of the Yellow River within the Budyko framework, *Journal of Hydrology*, *558*, 301-313. https://doi.org/10.1016/j.jhydrol.2018.01.050

Wang, Z., Xu, M., Liu, X., Singh, D. K., and Fu, X. (2022), Quantifying the impact of climate change and anthropogenic activities on runoff and sediment load reduction in a typical Loess Plateau watershed, *Journal of Hydrology: Regional Studies*, *39*. https://doi.org/10.1016/j.ejrh.2022.100992

Wu, J., Miao, C., Yang, T., Duan, Q., and Zhang, X. (2018), Modeling streamflow and sediment responses to climate change and human activities in the Yanhe River, China, *Hydrology Research*, *49*(1), 150-162. https://doi.org/10.2166/nh.2017.168

Xin, Y., Yang, Y., Chen, X., Yue, X., Liu, Y., and Yin, C. (2022), Evaluation of IMERG and ERA5 precipitation products over the Mongolian Plateau, *Sci Rep*, *12*(1), 21776. https://doi.org/10.1038/s41598-022-26047-8

Xu, J., Ma, Z., Yan, S., and Peng, J. (2022), Do ERA5 and ERA5-land precipitation estimates outperform satellite-based precipitation products? A comprehensive comparison between state-of-the-art model-based and satellite-based precipitation products over mainland China, *Journal of Hydrology*, *605*. https://doi.org/10.1016/j.jhydrol.2021.127353

Xu, X., Yang, D., Yang, H., and Lei, H. (2014), Attribution analysis based on the Budyko hypothesis for detecting the dominant cause of runoff decline in Haihe basin, *Journal of Hydrology*, *510*, 530-540. https://doi.org/10.1016/j.jhydrol.2013.12.052

Yang, D., Herath, S., and Musiake, K. (2000), Comparison of different distributed hydrological models for characterization of catchment spatial variability, *Hydrological Processes*, *14*(3), 403-416. https://doi.org/10.1002/(sici)1099-1085(20000228)14:3<403::Aid-hyp945>3.0.Co;2-3

Yang, D., Li, C., Hu, H., Lei, Z., Yang, S., Kusuda, T., Koike, T., and Musiake, K. (2004), Analysis of water resources variability in the Yellow River of China during the last half century using historical data, *Water Resources Research*, *40*(6). https://doi.org/10.1029/2003wr002763

Yang, H., Yang, D., Lei, Z., and Sun, F. (2008), New analytical derivation of the mean annual water-energy balance equation, *Water Resources Research*, *44*(3). https://doi.org/10.1029/2007wr006135

Zhao, G., Mu, X., Jiao, J., Gao, P., Sun, W., Li, E., Wei, Y., and Huang, J. (2018), Assessing response of sediment load variation to climate change and human activities with six different approaches, *Science of the Total Environment*, *639*, 773-784. https://doi.org/10.1016/j.scitotenv.2018.05.154

Zhou, Y., et al. (2023), Ecological restoration exacerbates the agriculture-induced water crisis in North China Region, *Agricultural and Forest Meteorology*, *331*. https://doi.org/10.1016/j.agrformet.2023.109341